


Microstructured layered targets for improved laser-induced x-ray backlightersS. Sander ^{1,*}, T. Ebert ¹, D. Hartnagel ¹, M. Hesse ¹, X. Pan ^{2,3}, G. Schaumann ¹, M. Šmíd ², K. Falk ^{2,3,4} and M. Roth ¹¹*Institut für Kernphysik, Fachbereich Physik, Technische Universität Darmstadt, 64289 Darmstadt, Germany*²*Helmholtz-Zentrum Dresden-Rossendorf, 01328 Dresden, Germany*³*Technische Universität Dresden, 01062 Dresden, Germany*⁴*Institute of Physics of the ASCR, 182 21 Prague, Czech Republic* (Received 1 March 2021; revised 26 August 2021; accepted 8 December 2021; published 27 December 2021)

We present the usage of two-layer targets with laser-illuminated front-side microstructures for x-ray backlighter applications. The targets consisted of a silicon front layer and copper back side layer. The structured layer was irradiated by the 500-fs PHELIX laser with an intensity above 10^{20} W cm⁻². The total emission and one-dimensional extent of the copper $K\alpha$ x-ray emission as well as a wide spectral range between 7.9 and 9.0 keV were recorded with an array of crystal spectrometers. The measurements show that the front-side modifications of the silicon in the form of conical microstructures maintain the same peak brightness of the $K\alpha$ emission as flat copper foils while suppressing the thermal emission background significantly. The observed $K\alpha$ source sizes can be influenced by tilting the conical microstructures with respect to the laser axis. Overall, the recorded copper $K\alpha$ photon yields were in the range of 10^{11} sr⁻¹, demonstrating the suitability of these targets for probing applications without subjecting the probed material to additional heating from thermal line emission.

DOI: [10.1103/PhysRevE.104.065207](https://doi.org/10.1103/PhysRevE.104.065207)**I. INTRODUCTION**

The interaction of a high-intensity short-pulse laser with a solid target is used to produce high temperature, near solid density plasma states. These states are of interest for studying high energy density (HED) physics as well as for generating energetic particle beams and short-pulse x-ray sources [1–3]. In particular, the spectral line emission of laser driven x-ray sources provides a unique tool for diagnostic applications in HED experiments [4–8]. These sources have been shown to provide sufficiently high photon numbers within a narrow bandwidth for spectrally resolved scattering measurements, such as x-ray Thomson scattering or Talbot-Lau interferometry [9–11], thereby giving insights into the temperature, density, and ionization state of the probed matter. Furthermore, laser driven x-ray sources have been widely used as high brightness backlighters for radiography of inertial confinement fusion and other HED experiments [12,13].

Past studies have investigated multiple aspects of these laser driven x-ray sources depending on the intended application. The primary interest in the optimization of laser-driven backlighters are the source size, overall photon yield, and conversion efficiency (CE) [11,12]. The x-ray energy is also important for probing large or dense samples. In particular, emission from higher-Z materials is more suitable for probing strongly heated and dense matter [12]. Investigations into the dependence of the CE on the target material have shown that thermal He α and Ly α line emission from highly ionized material decreases the CE with increasing Z [14,15], while $K\alpha$ emission from weakly ionized, cold material has shown a

near independence of CE from Z [9]. The highly nonuniform plasma produced during the laser-matter interaction with a simple flat foil target also results in a complex emission spectrum ranging from cold $K\alpha$ line emission to He α and Ly α emission from the heated interaction region, with the possibility of multiple red-shifted satellite lines. For applications that rely on a small spectral bandwidth, such as scattering experiments [5–8], the absence of prominent satellite lines in weakly ionized $K\alpha$ sources is preferred over thermal He α and Ly α sources [9].

In order to achieve a clean spectrum without thermal line emission, layered targets consisting of two different materials are used [16]. The front layer interacts with the laser and is strongly heated. The accelerated electrons travel into the back side layer that is still relatively cold and therefore produces a pure $K\alpha$ emission without any heating effects. A high-quality $K\alpha$ source can be achieved by carefully choosing a material with no prominent lines within the considered $K\alpha$ spectrum of the back side layer. However, as energy is already deposited in the front layer, a lower photon yield is to be expected from the back side layer. Changing the laser-target interaction can counterbalance this effect. Research has investigated the enhancement of the laser-target coupling through foams [17], nanostructures [18], and subwavelength gratings [19] to improve the x-ray emission directly. More recently, front-side modifications in the form of μ m-scale, conical structures [20] have shown a strong increase of the x-ray photon yield. This approach has the additional advantage that the back side layer can be limited in mass and further customized. This allows us to tailor the target with respect to increased photon yield or limited source size.

In this work, targets consisting of a silicon (Si) front surface and a copper (Cu) back side are investigated. The

*Corresponding author: ssander@ikp.tu-darmstadt.de

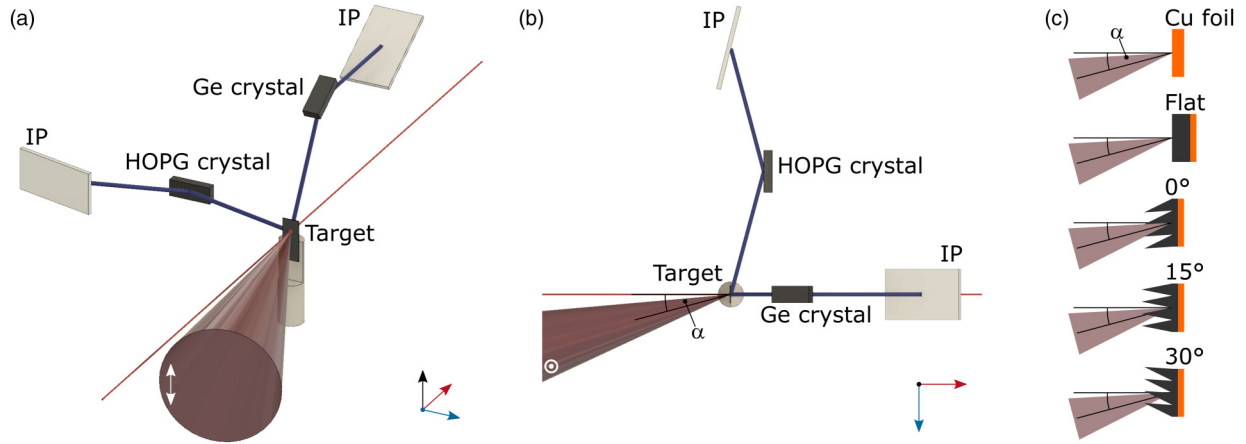


FIG. 1. Experimental setup in side (a) and top (b) view, as well as schematics of the studied targets (c). The PHELIX laser is focused onto the layered target under $\alpha = 15^\circ$ to target normal (red solid line). The laser polarization with respect to a flat foil target (s-pol) is indicated in white. Two spectrometers observe the x-ray emission on the target back side. A HOPG crystal is positioned in the laser plane, whereas a Ge crystal is pointing upwards but in target normal direction. The layered targets consist of a Si front side (black) and a Cu back side (orange). The target names describe the angular difference between structure axis and laser axis.

experiments were performed at the PHELIX laser facility in Darmstadt, Germany [21]. The setup, used diagnostics and targets are described in Sec. II. The benefit of the layered targets with respect to their spectral quality is shown in contrast to a pure Cu foil in Sec. III A. Furthermore, the enhancement by microstructured front surfaces is presented. Recorded photon numbers, conversion efficiencies, and source sizes are discussed in Secs. III B and III C.

II. EXPERIMENTAL SETUP AND DIAGNOSTICS

The general setup of the high-intensity campaign is displayed in Fig. 1. The laser beam with a wavelength of 1053 nm and an average energy of (146 ± 23) J was focused onto the target with a Cu off-axis parabolic mirror down to a focal spot size of (6.4 ± 1.2) μm [full width at half maximum (FWHM)] for all measurements. The focal imaging displayed a comalike aberration around the focal spot, such that only about 40% of the laser energy was contained in the focal spot with an area of (32 ± 12) μm^2 FWHM. The laser pulse length was 500 fs, resulting in mean peak intensity on target of $(3.4 \pm 1.2) \times 10^{20}$ W cm^{-2} . The large uncertainty in this intensity is derived from the shot-to-shot energy variation during the campaign and slight changes in the best achievable focal spot. The laser incidence angle was 15° with respect to the target normal and had a contrast of 10^{12} between the amplified spontaneous emission level and peak power [22–24]. The Rayleigh length of the PHELIX laser in our experimental setup was measured to be 35 μm , which gives a relatively wide margin for target positioning.

Multiple spectrometers were used to measure the time-integrated x-ray spectra emitted from the targets, two of which will be used for this analysis and further described. Both recorded the x-ray emission from the target back side as displayed in Fig. 1. A 20- μm -thick black polycarbonate film was used as a debris shield protecting each crystal and to keep the image plate (IP) packs light tight. Two-millimeter-thick Pb plates were used to screen the direct line of sight to the laser interaction area to reduce the hard x-ray background. The IPs

were scanned with a Typhoon FLA 7000 scanner approximately 20 min after the laser shot. The dispersion relation for the spectrometers was found by a second order polynomial fit to known line positions in the spectrum.

One of the spectrometers contained a flat highly oriented pyrolytic graphite (HOPG) crystal as the diffractive element [25]. This mosaic crystal features a high reflectivity due to mosaic focusing but has a reduced resolution due to the angular spread of the crystallites. With a large crystal surface of 20×50 mm^2 , the spectrometer was used to image the spectral range between 7.9 and 9.0 keV. The spectral range was chosen to record the Cu $K\alpha$ and $K\beta$ as well as the He α and Ly α line emission. It covered a solid angle of 2.9×10^{-3} sr and was aligned at 41° with respect to target normal. The used IP was a Fujifilm BAS-SR.

The second spectrometer was set up with a toroidally curved germanium (Ge) crystal with a surface area of 15×50 mm^2 [26]. The spectral range was set to 8.0 to 8.1 keV, imaging the Cu $K\alpha$ emission with a solid angle of 3.9×10^{-3} sr on a Fujifilm BAS-TR IP. In addition, the geometry of the crystal enabled spatial imaging of the source with a resolution of 18 μm perpendicular to the dispersive direction. The spectrometer was positioned at an angle of 64° to target normal.

Three types of targets were used, namely plain Cu targets, flat layered targets and microstructured layered targets. Figure 1(c) shows schematics of these targets. To obtain a reference spectrum, foils of pure Cu with 10 μm thickness were employed. The layered targets consisted of a Si front side with a Cu layer on the back side. Flat targets were produced from a 15- μm -thick Si wafer with a 5- μm -thick layer of Cu deposited on the back side using thermal evaporation. The thickness of the Si wafer was chosen to correlate with the line density of the subsequently described microstructured targets.

For the front surface modified targets, a comparable 5- μm -thick layer of Cu was deposited via thermal evaporation onto one side of a polished Si wafer. Then the Si wafer was repetitively irradiated on the other side by a series of femtosecond laser pulses to produce conical microstructures. The

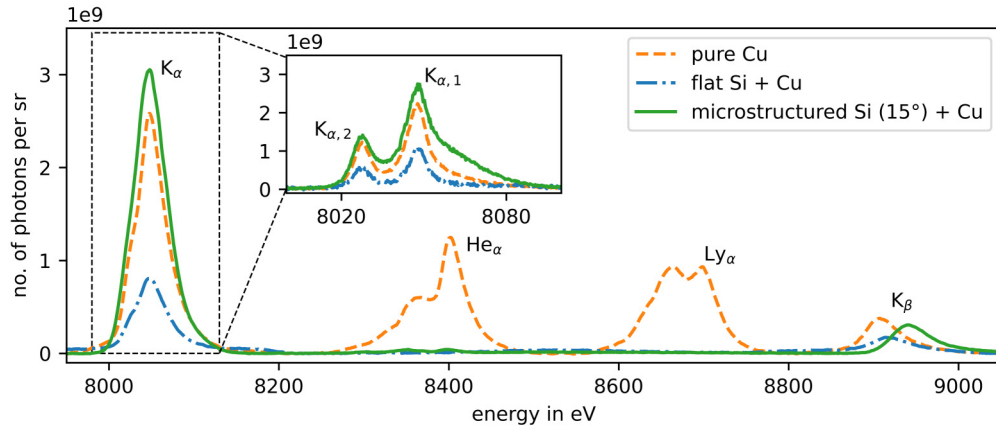


FIG. 2. Spectra of a pure Cu foil (orange dashed), a flat Si wafer with Cu back side (blue dash-point) and microstructured Si wafer with Cu back side (green solid) measured with the HOPG spectrometer. The pure Cu foil exhibits multiple line emissions, both from cold, unionized material ($K\alpha$ and $K\beta$) as well as highly ionized atoms. The two layered targets show no heating effects, demonstrating the effective decoupling of direct laser heating and x-ray emission. Through improvement of the laser interaction with the target by using a microstructured front, the decrease in efficiency in $K\alpha$ line emission of the decoupling can be negated. The inset displays spectra recorded by the toroidal Ge spectrometer for the same shots. The $K\alpha_1$ and $K\alpha_2$ line emission can be clearly distinguished. The much higher spectral resolution of the Ge spectrometer also allows for a better resolution of the blue wing between 8060 and 8080 eV in comparison to the HOPG spectrometer.

dimensions of the resulting structures are $25\text{-}\mu\text{m}$ cones with a base width of $6\text{ }\mu\text{m}$. The remaining substrate between cone base and Cu layer was $5\text{ }\mu\text{m}$. In one configuration, the microstructures are oriented along the target normal and interact with the high-intensity laser under its pointing angle of 15° . Tilted microstructures with a 0° and 30° angle with respect to the high-intensity laser were also produced by tilting the substrate during the structuring process, as shown in Fig. 1(c). Further information on these microstructured targets and their fabrication from Si can be found in publications by Ebert *et al.* [27,28].

Additionally, for a subset of both flat and structured layered targets, the deposited Cu material was limited to two $(100 \pm 10)\text{-}\mu\text{m}$ -diameter dots. These dots were spaced $(250 \pm 10)\text{ }\mu\text{m}$ center to center. All targets were produced at the Detector and Target Laboratory, Institute for Nuclear Physics, Technical University Darmstadt.

III. RESULTS AND DISCUSSION

A. Spectral features

Multiple K -shell line emissions from different ionization states can be observed during a laser-matter interaction and are a useful tool to investigate the plasma conditions. The interaction of the laser with the front side material results in a high temperature and the generation of energetic electrons, usually referred to as *hot* or *fast* electrons. K -shell vacancies are generated by inelastic collisions of these hot electrons. Different characteristic emission is observed depending on the plasma conditions. If the bulk material is still relatively cold and the atoms are weakly ionized, the characteristic inner-shell $2p\text{-}1s$ transition lines are observed, commonly referred to as cold $K\alpha$ lines [29]. With increasing number of collisions from bulk electrons, the outer shells are ionized, and M -shell vacancies occur. As a result, the electronic screening of the K and L shells decreases and a broadening and blueshift of the *cold* $K\alpha$ lines can be observed [30]. In addition,

the heated plasma formed on the front surface contains an increasing mixture of ionization states, therefore a variety of shifted transitions can be observed. For a strongly heated target, the most prominent lines include emission from Li-like ($\text{Li}\alpha$), He-like ($\text{He}\alpha$), and H-like ($\text{Ly}\alpha$) states [31,32].

Figure 2 displays time-integrated spectra of three measurements of the different target types. The spectrum of the pure Cu target shows multiple distinct emission lines. On the left and right sides of the spectrum, the $K\alpha$ and $K\beta$ lines are visible. The $K\alpha$ emission is expected to occur during the initial interaction phase before the laser reaches its peak and toward the back side of the target, where the bulk material is still cold. Together with this cold material emission, $\text{Li}\alpha$, $\text{He}\alpha$, and $\text{Ly}\alpha$ lines can be seen in the spectrum. As the $\text{He}\alpha$ and $\text{Ly}\alpha$ peaks are of a similar intensity, we infer a temperature in the order of 1 to few keV [33].

For the flat, layered target cold material emission is observed as well. However, the $K\alpha$ signal is substantially decreased by approximately 70% compared to the emission recorded for the pure Cu foil. In part, this reduced emission can be attributed to the additional collisions of the electrons inside the Si region of the target. The cross sections for electron impact K -shell ionization in Cu rises sharply above the binding energy of 8.979 keV, has a maximum around 30 keV and then falls again to energies of 1 MeV [34]. While hot electron temperatures of up to a few MeV are observed for laser intensities exceeding $1 \times 10^{20}\text{ W cm}^{-2}$, most electrons are expected to have energies in the order of a few 100 keV [35,36]. According to the continuous slowing down approximation, electrons with energies below 38 keV are completely stopped in the Si layer at the target front. Consequently, these low-energy electrons do not contribute to K -shell ionization. Of the remaining electrons, only those that enter the Cu layer with a residual energy below 44 keV completely deposit their energy in the $5\text{-}\mu\text{m}$ -thick back side layer. This leaves a large portion of electrons which only deposit part of their energy and primarily contribute to the K -shell ionization through

refluxing [35]. Compared to the 10- μm -thick flat foil, this significantly reduces the overall available energy for K -shell ionization in the 5- μm -thick Cu back side of the layered target and thus explains the observed reduction of $K\alpha$ emission. As we did not measure the target performance as a function of the Cu layer thickness, the reduction in emission as a function of this parameter cannot be quantified at this point. Based on this reasoning, we conclude that the decreased $K\alpha$ signal is mainly the result of energy losses inside the Si region of the target and the target performance might be further increased with a thicker back side Cu layer.

No emission of a heated plasma is seen with the flat layered target. As the laser only interacts directly with the Si, there is no substantial heating of Cu during the laser pulse. Theobald *et al.* have shown that this strong heating is localized to a small surface region of about 1- μm thickness for intensities above $10^{19} \text{ W cm}^{-2}$ [16].

For a 15° microstructured front surface, mainly cold K -shell emission is observed as well. However, the $K\alpha$ signal height is increased by a factor of 3.5 when compared with the flat layered target, up to the level of the pure Cu foil. As the line density for both the flat and microstructured target was chosen to be the same, electrons experience on average the same amount of collisions inside the Si before interacting with the Cu. From this follows, that the electron distribution for the microstructured targets is changed toward higher numbers and energies, which is a result of a changed laser-target interaction. In a similar experiment conducted at the VULCAN laser system by Ebert *et al.* [20], similar microstructured Si foils were used without a secondary layer. Observation of the Si emission displayed a strong increase over the complete Si spectrum together with a higher electron flux, while the measured electron temperature change only slightly. This is in good agreement with our findings. Even though the electron distribution is changed substantially in the Si layer of the target, still no thermal emission is observed for the Cu layer.

The inset in Fig. 2 displays the observed spectra of the same measurements from the Ge spectrometer. The two transitions $K\alpha_1$ and $K\alpha_2$ can be clearly distinguished. The observed trend in their intensities closely matches the HOPG spectrometer. This is to be expected as the emission of K -shell radiation is isotropic. To infer rough temperatures of the bulk electrons, the atomic kinetics model SCFLY [37] was used to model the spectral emission from a Cu slab of 5 μm thickness. As the strongly heated area of the layered target is localized within the Si layer [16], we expect no substantial change in density of the Cu layer during the x-ray emission and therefore assume solid density for the calculations. The K -shell ionization is driven by a secondary hot electron component. We found no strong correlation of the calculated spectra with the hot electron temperature in the range of 0.5–10 MeV and assumed a temperature of 1 MeV with a share of 0.1 % of the overall electron population. The calculated spectra were then convolved with an instrumental function with a width of 1.8 eV. As the measured spectra are time integrated, a single temperature, single density calculation is only an indication of the time-averaged conditions. This calculation was found through minimization of the arithmetic distance between the measured and calculated spectra. Typically, this approach yielded a reasonable fit for one temperature, but the blue wing

emission between 8050 and 8090 eV was underestimated by this approach. Therefore, we combined multiple simulations with different scaling factors to best represent the complete observed spectra.

The measured spectra are plotted together with the best fitting temperature calculations in Fig. 3. For the flat layered target [Fig. 3(a)], the model with a bulk electron temperature of 30 eV resulted in the best fit. Adding a second component with a higher temperature of 90 eV increased the fit toward the blue wing of the $K\alpha_1$ peak. For the microstructured targets, this blue wing is much more developed. While the base peak shape can be represented with a slightly higher temperature of 40 eV, additional components between 90 and 160 eV are required to match the measured spectrum, indicating a strong ionization of the Cu up to approximately Cu^{16+} . The temperatures stated here do not represent the full picture but rather indicate a temperature range in which the material was and are only used to estimate an upper limit of the temperature. We infer from this analysis that the bulk electron temperatures of the Cu layer was a few tens of eV and stayed below 200 eV. We expect that the observed stronger ionization of the Cu layer in the case of the microstructured target is again a result of the increased collisions due to the higher electron numbers.

To summarize, suppression of the heating lines was observed for flat layered targets but resulted in a strong decrease in $K\alpha$ yield. The microstructured front surfaces counteract this decrease and result in the same $K\alpha$ yield as the pure Cu foils, while the heating lines are suppressed at the same time.

B. Photon yield and conversion efficiency

The raw signal is given in units of photostimulated luminescence since the spectra were recorded with IPs. The absolute signal detected in terms of number of photons emitted per sr was obtained through a series of conversions. As the signal on an IP fades with time, the data are corrected with the fading functions for both IP types found by Boutoux *et al.* [38]. The response function of Fuji IPs was taken from Meadowcroft *et al.* [39]. For the mosaic HOPG crystal, the spectrometer efficiency was estimated by the ray-tracing code mmpxrt [40], while the Ge crystals reflectivity was calculated with the DIXI code [41]. The filter transmission is estimated with values given by Henke *et al.* [42].

With the above-mentioned conversions, the photon numbers per sr integrated over 0.5% bandwidth (BW) around the $K\alpha$ peak during the experiment can be calculated and are summarized in Table I. The overall photon yield is very similar between the pure Cu foil and the microstructured layered targets with the closest agreement between the pure Cu foil and the 15° tilted microstructures. For structures facing into the laser axis (0° targets), the yield is slightly decreased, while for the 30° targets the highest photon yield of $(5.4 \pm 2.7) \times 10^{11} \text{ ph sr}^{-1}$, which corresponds to $(3.7 \pm 1.8) \times 10^{11} \text{ ph J}^{-1} \text{ sr}^{-1}$, was recorded. We expect this increase in photon yield is in part a result of the changing source size, summarized in Table I as well, which will be further discussed in Sec. III C. The measured photon numbers agree well with other works, reporting similar yields in the range of $10^9 \text{ ph sr}^{-1} \text{ J}^{-1}$ [43]. In comparison, the flat front surfaced target shows only about half the photon number observed.

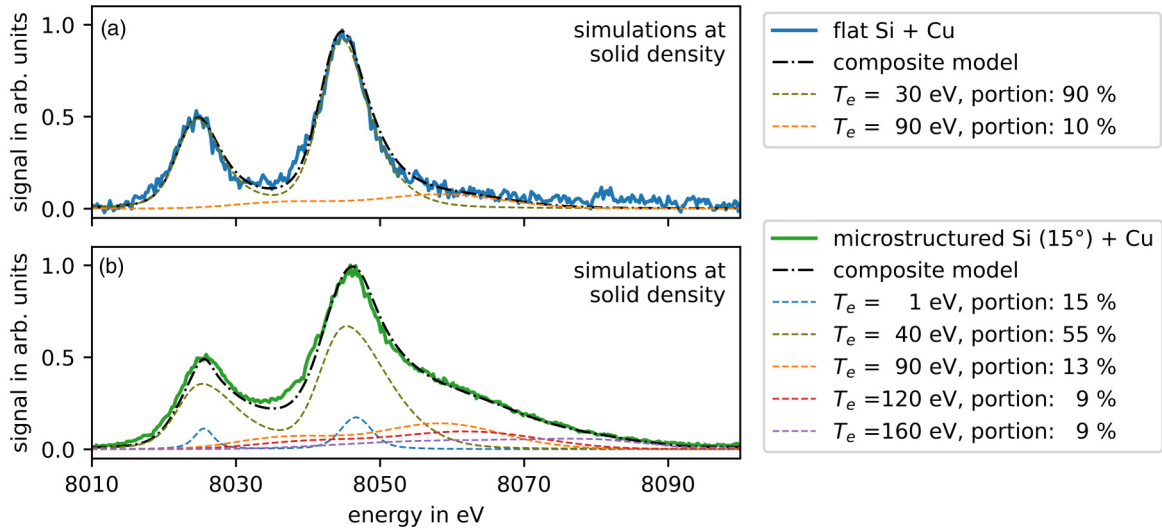


FIG. 3. Comparison of normalized, measured spectra with calculated spectra for (a) a flat layer target and (b) a microstructured layer target. The measured spectra are the same as shown in the inset of Fig. 2. The calculations were made with the atomic kinetics code SCFLY. To model the blue wing emission between 8050 and 8090 eV, additional components between 90 and 160 eV are included. The different components are scaled and then added to derive a composite model, where the various scaling factors can be thought of as the portion of material in this condition.

Equally of interest is the CE, defined by the energy in x-ray photons normalized to the energy delivered by the laser. The CEs are calculated for a 0.5% BW around the $K\alpha$ peak and are summarized in Table I. The CE of the pure Cu foil and the microstructured targets is very similar and exceeds the CE of the flat foil by a factor of 2 to 3. We attribute this enhanced performance of the microstructured targets in contrast to the flat layered targets to the improved laser coupling already discussed in Sec. III A and by Ebert *et al.* [20]. On the whole, the CE of about $(40.0 \pm 2.0) \times 10^{-6} \text{ sr}^{-1}$ is lower than the values of up to $1.2 \times 10^{-5} \text{ sr}^{-1}$ reported by other groups studying Cu targets at similar intensities [35]. Works by Theobald *et al.* and Neumayer *et al.* [16,35] showed the importance of electron refluxing on the CE for intensities beyond $10^{18} \text{ W cm}^{-2}$ for the emission of $K\alpha$ radiation. For large targets with low electron refluxing capabilities, the $K\alpha$ CE decreases rapidly with increasing intensity. As the targets investigated during this study were roughly $1.5 \times 5 \text{ mm}^2$ in lateral dimensions and mounted on a 6-mm-diameter polystyrol stalk, we expect the

electron refluxing was limited, resulting in the lowered CE. Limiting the targets lateral dimensions should improve the refluxing capabilities and an enhanced CE is to be expected.

C. Source sizes

The source sizes were measured with the Ge spectrometer by fitting a Gaussian peak profile along the spatial axis of the recorded $K\alpha_1$ peak. With the magnification of the spectrometer, which was calculated with the ray-tracing code mmpxrt [40], the source sizes are inferred for all layered targets and are displayed in Fig. 4 and Table I. The source size is much larger than the original laser spot for all layered targets. Even including the observed comalike features around the laser focus, the source size is approximately 8 times larger than the laser spot for the flat target. For the microstructured targets facing away from the laser axis (15°), the source size is slightly increased in comparison with the flat target. This is to be expected, as the rough surface increases the interaction area of the

TABLE I. Measured photon numbers in a 0.5% BW around the $K\alpha$ peak, laser energies, corresponding conversion efficiencies, source sizes, and photon fluxes for the investigated target types. The structured targets increase the photon yield to the same level as a pure Cu foil. The conversion efficiency is similar for all structured targets when compared to the pure Cu foil and increased by a factor of 2–3 in comparison with the flat layered target. The source size is relatively large for all layered targets. A decrease is observed for 0° targets. All values are derived from single shot measurements. For all microstructured targets, the values are derived from the mean of two measurements for the specific configuration.

Target type	No. of photons in 10^{11} sr^{-1}	Laser energy in J	CE in 10^{-6} sr^{-1}	Source size in μm	No. of photons in $10^{13} \text{ sr}^{-1} \text{ mm}^{-2}$
Pure Cu foil	4.8 ± 2.4	155 ± 2	4.0 ± 2.0	—	—
Flat Si + Cu	2.0 ± 1.0	160 ± 18	1.6 ± 0.8	155.6 ± 1.9	1.1 ± 0.6
0° struct Si + Cu	3.8 ± 1.9	125 ± 8	4.0 ± 2.0	138.6 ± 1.2	2.5 ± 0.6
15° struct Si + Cu	4.6 ± 2.3	163 ± 13	3.6 ± 1.8	161.0 ± 1.3	2.2 ± 0.5
30° struct Si + Cu	5.4 ± 2.7	146 ± 12	4.8 ± 2.4	197.0 ± 5.0	1.8 ± 0.7

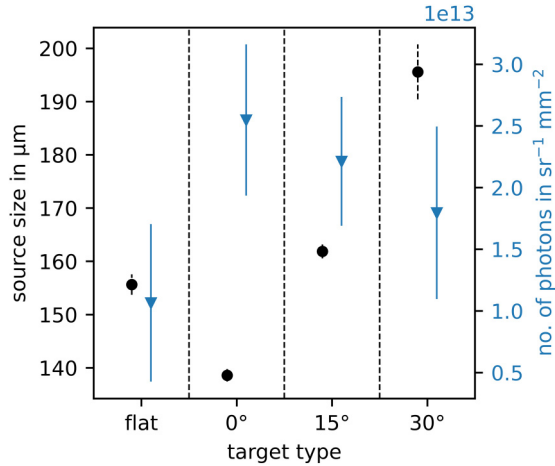


FIG. 4. Source sizes (black circle) and estimated brilliances (blue triangle). The source sizes (FWHM) of the investigated targets are much larger than the laser spot. The source size increases slightly for structured targets compared to flat targets as expected (target types 15° and 30°). A tilt of the microstructures (target type 0°) into the laser axis, however, shows a clear decrease in source size which can be explained geometrically. The photon flux is increased for the 0° target.

laser. For the 30° microstructures, this effect further increases and subsequently also increases the photon yield as mention in Sec. III B. On the other hand, microstructures pointing along the laser axis focus the laser, resulting in an overall smaller source size and slight decrease in $K\alpha$ photon yield (see Table I). However, normalizing the photon yield to the measured source size, as displayed in Fig. 4 and Table I, shows a varying photon flux from the differently tilted microstructure targets, with a maximum for the 0° tilted microstructures. We expect that with the change of tilt angle the location of the electron generation inside the region of the microstructures also changes. For the 0° target, the laser can penetrate deeper into a needle valley and the hot electrons produced there experience less collisions before interacting with the Cu back side layer. On the other hand, for the 30° target, the laser interacts more with the needle tips and the electrons have to move through more material before reaching the Cu back side layer, broadening due to an increased amount of collisions.

For layered targets with two Cu dots, two separate sources can clearly be distinguished on the IP of the toroidal spectrometer, as shown in Fig. 5. Limiting the emission material on the back side decreases the source size to roughly $(107 \pm 10) \mu\text{m}$ (FWHM), agreeing well with the initial dot sizes of $(100 \pm 4) \mu\text{m}$. The separation of the sources is slightly smaller at $(205 \pm 10) \mu\text{m}$ in comparison to the initial center to center distance of $(242 \pm 10) \mu\text{m}$. We attribute this discrepancy to a slight rotation of the target plane with respect to the spatial imaging axis, resulting in an apparent smaller spacing between the two sources. Other studies have investigated wire targets or foils, which are irradiated edge-on, to limit the source size at least in one dimension down to a few microns [12]. The targets presented here pose the possibility to limit the source size in two dimensions while retaining the advantages described above for the layered targets, such

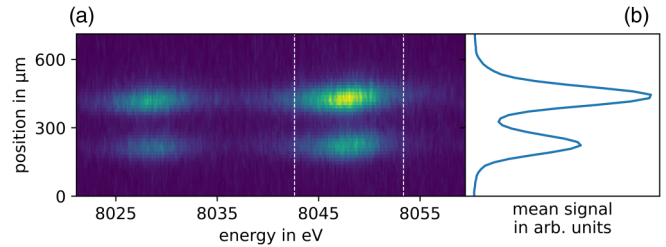


FIG. 5. Observed spectra of a two dot target as recorded with an IP (a) and the corresponding spatial distribution of the $K\alpha_1$ line (b). The distinction between the two dots acting as sources is clearly visible. The FWHM of a Gaussian fit is approximately $(107 \pm 10) \mu\text{m}$ for both sources. This is in good agreement with the initial Cu dot size of $(100 \pm 4) \mu\text{m}$. The separation is found to be $(205 \pm 10) \mu\text{m}$, which is smaller than the initial target design.

as a suppression of thermal emission and an increased yield through front side modifications. The next step toward a pointlike brilliant $K\alpha$ backlighter source would be a material deposition of a much smaller volume. In addition, as the laser interaction is decoupled from the emission material, multiple emitting materials on the back side on an enhancing front side could be realized. This opens the possibility to probe experiments with multiple different $K\alpha$ lines of varying energy.

IV. CONCLUSION

We present the high-quality spectral output of layered targets for x-ray source applications at high-power laser facilities. Diminishing photon yields due to the layered structure are compensated with the enhancement of the laser-target coupling through front-side microstructures from $(2.0 \pm 1.0) \times 10^{11} \text{ph sr}^{-1}$ up to $(5.4 \pm 2.7) \times 10^{11} \text{ph sr}^{-1}$. The thermal line emission typically observed for directly driven one-material x-ray backlighters is suppressed significantly, resulting in pure $K\alpha$ sources for probing applications. A tilt of the conical microstructures with respect to the laser axis increases both the total photon yield and source size with increasing angles ranging from 0° to 30° . The highest photon flux is achieved with the 0° targets that point in the direction of the incoming laser, reaching $2.5 \pm 0.6) \times 10^{13} \text{ph sr}^{-1} \text{mm}^{-2}$. The source size can be limited through defined material deposition, in our case to $100 \mu\text{m}$ diameter. The resulting $K\alpha$ spectrum is of high quality and brilliance for $K\alpha$ spectroscopic applications, without the presence of satellite or thermal line emission.

ACKNOWLEDGMENTS

The authors thank A. Tebartz of the Institute of Nuclear Physics at the Technical University of Darmstadt, as well as P. Perez-Martin of the Helmholtz-Zentrum Dresden-Rossendorf and the whole PHELIX team at GSI for their support during the experimental campaign. We also thank D. Montgomery from the Los Alamos National Laboratory for providing the Ge crystal. This project was financially supported by the BMBF (Project No. 05P19RDF A1), by the Hessian LOEWE initiative within the Nuclear Photonics project at TU Darmstadt, and by the DFG in the framework of the Excellence

Initiative, Darmstadt Graduate School of Excellence Energy Science and Engineering (GSC 1070). This research was also

supported by the Helmholtz Association under Grant No. VH-NG-1338.

- [1] G. A. Mourou, T. Tajima, and S. V. Bulanov, Optics in the relativistic regime, *Rev. Mod. Phys.* **78**, 309 (2006).
- [2] R. A. Snavely, M. H. Key, S. P. Hatchett, T. E. Cowan, M. Roth, T. W. Phillips, M. A. Stoyer, E. A. Henry, T. C. Sangster, M. S. Singh, S. C. Wilks, A. MacKinnon, A. Offenberger, D. M. Pennington, K. Yasuike, A. B. Langdon, B. F. Lasinski, J. Johnson, M. D. Perry, and E. M. Campbell, Intense High-Energy Proton Beams from Petawatt-Laser Irradiation of Solids, *Phys. Rev. Lett.* **85**, 2945 (2000).
- [3] C. Reich, P. Gibbon, I. Uschmann, and E. Förster, Yield Optimization and Time Structure of Femtosecond Laser Plasma $K\alpha$ sources, *Phys. Rev. Lett.* **84**, 4846 (2000).
- [4] J. Workman, M. Nantel, A. Maksimchuk, and D. Umstadter, Application of a picosecond soft x-ray source to time-resolved plasma dynamics, *Appl. Phys. Lett.* **70**, 312 (1997).
- [5] S. H. Glenzer, G. Gregori, R. W. Lee, F. J. Rogers, S. W. Pollaine, and O. L. Landen, Demonstration of Spectrally Resolved X-Ray Scattering in Dense Plasmas, *Phys. Rev. Lett.* **90**, 175002 (2003).
- [6] S. H. Glenzer, G. Gregori, F. J. Rogers, D. H. Froula, S. W. Pollaine, R. S. Wallace, and O. L. Landen, X-ray scattering from solid density plasmas, *Phys. Plasmas* **10**, 2433 (2003).
- [7] S. H. Glenzer, O. L. Landen, P. Neumayer, R. W. Lee, K. Widmann, S. W. Pollaine, R. J. Wallace, G. Gregori, A. Höll, T. Bornath, R. Thiele, V. Schwarz, W. D. Kraeft, and R. Redmer, Observations of Plasmons in Warm Dense Matter, *Phys. Rev. Lett.* **98**, 065002 (2007).
- [8] K. Falk, C. L. Fryer, E. J. Gamboa, C. W. Greeff, H. M. Johns, D. W. Schmidt, M. Šmíd, J. F. Benage, and D. S. Montgomery, X-ray Thomson scattering measurement of temperature in warm dense carbon, *Plasma Phys. Control. Fus.* **59**, 014050 (2017).
- [9] S. H. Glenzer and R. Redmer, X-ray Thomson scattering in high energy density plasmas, *Rev. Mod. Phys.* **81**, 1625 (2009).
- [10] A. L. Kritcher, P. Neumayer, M. K. Urry, H. Robey, C. Niemann, O. L. Landen, E. Morse, and S. H. Glenzer, K-alpha conversion efficiency measurements for X-ray scattering in inertial confinement fusion plasmas, *High Energy Density Phys.* **3**, 156 (2007).
- [11] V. Bouffetier, L. Ceurvorst, M. P. Valdivia, F. Dorchie, S. Hulin, T. Goudal, D. Stutman, and A. Casner, Proof-of-concept Talbot-Lau x-ray interferometry with a high-intensity, high-repetition-rate, laser-driven K-alpha source, *Appl. Opt.* **59**, 8380 (2020).
- [12] H.-S. Park, D. M. Chambers, H.-K. Chung, R. J. Clarke, R. Eagleton, E. Giraldez, T. Goldsack, R. Heathcote, N. Izumi, M. H. Key, J. A. King, J. A. Koch, O. L. Landen, A. Nikroo, P. K. Patel, D. F. Price, B. A. Remington, H. F. Robey, R. A. Snavely, D. A. Steinman *et al.*, High-energy $K\alpha$ radiography using high-intensity, short-pulse lasers, *Phys. Plasmas* **13**, 056309 (2006).
- [13] H. S. Park, B. R. Maddox, E. Giraldez, S. P. Hatchett, L. T. Hudson, N. Izumi, M. H. Key, S. Le Pape, A. J. MacKinnon, A. G. MacPhee, P. K. Patel, T. W. Phillips, B. A. Remington, J. F. Seely, R. Tommasini, R. Town, J. Workman, and E. Brambrink, High-resolution 17-75 keV backlighters for high energy density experiments, *Phys. Plasmas* **15**, 072705 (2008).
- [14] J. Workman and G. A. Kyrala, X-ray yield scaling studies performed on the OMEGA laser, *Rev. Sci. Instrum.* **72**, 678 (2001).
- [15] L. E. Ruggles, J. L. Porter, P. K. Rambo, W. W. Simpson, M. F. Vargas, G. R. Bennett, and I. C. Smith, Measurements of 4-10 keV x-ray production with the Z-Beamlet laser, *Rev. Sci. Instrum.* **74**, 2206 (2003).
- [16] W. Theobald, K. Akli, R. Clarke, J. A. Delettrez, R. R. Freeman, S. Glenzer, J. Green, G. Gregori, R. Heathcote, N. Izumi, J. A. King, J. A. Koch, J. Kuba, K. Lancaster, A. J. MacKinnon, M. Key, C. Mileham, J. Myatt, D. Neely, P. A. Norreys *et al.*, Hot surface ionic line emission and cold K-inner shell emission from petawatt-laser-irradiated Cu foil targets, *Phys. Plasmas* **13**, 043102 (2006).
- [17] W. Shang, J. Yang, W. Zhang, Z. Li, B. Deng, Y. Dong, T. Zhu, C. Huang, X. Zhan, Y. Mei, L. Guo, R. Yu, S. Li, S. Jiang, S. Liu, F. Wang, Y. Ding, B. Zhang, and R. Betti, Experimental demonstration of laser to x-ray conversion enhancements with low density gold targets, *Appl. Phys. Lett.* **108**, 064102 (2016).
- [18] M. A. Purvis, V. N. Shlyaptsev, R. Hollinger, C. Bargsten, A. Pukhov, A. Prieto, Y. Wang, B. M. Luther, L. Yin, S. Wang, and J. J. Rocca, Relativistic plasma nanophotonics for ultrahigh energy density physics, *Nat. Photon.* **7**, 796 (2013).
- [19] S. Kahaly, S. K. Yadav, W. M. Wang, S. Sengupta, Z. M. Sheng, A. Das, P. K. Kaw, and G. R. Kumar, Near-Complete Absorption of Intense, Ultrashort Laser Light by Sub- λ gratings, *Phys. Rev. Lett.* **101**, 145001 (2008).
- [20] T. Ebert, N. W. Neumann, L. N. K. Döhl, J. Jarrett, C. Baird, R. Heathcote, M. Hesse, A. Hughes, P. McKenna, D. Neely, D. Rusby, G. Schaumann, C. Spindloe, A. Tebartz, N. Woolsey, and M. Roth, Enhanced brightness of a laser-driven x-ray and particle source by microstructured surfaces of silicon targets, *Phys. Plasmas* **27**, 043106 (2020).
- [21] P. Neumayer, R. Bock, S. Borneis, E. Brambrink, H. Brand, J. Caird, E. M. Campbell, E. Gaul, S. Goette, C. Haefner, T. Hahn, H. M. Heuck, D. H. Hoffmann, D. Javorkova, H. J. Kluge, T. Kuehl, S. Kunzer, T. Merz, E. Onkels, M. D. Perry *et al.*, Status of PHELIX laser and first experiments, *Laser Part. Beams* **23**, 385 (2005).
- [22] B. Aurand, Untersuchungen zu Mechanismen der Laser-Teilchenbeschleunigung, Ph.D. thesis, Johannes Gutenberg-Universität, 2012.
- [23] V. A. Schanz, Zeitlicher Laserpulscontrast - Metrologie und Optimierung, Ph.D. thesis, Technische Universität Darmstadt, 2019.
- [24] V. A. Schanz, C. Brabetz, D. J. Posor, D. Reemts, M. Roth, and V. Bagnoud, High dynamic range, large temporal domain laser pulse measurement, *Appl. Phys. B: Lasers Opt.* **125**, 61 (2019).
- [25] H. Legall, H. Stiel, M. Schnürer, M. Pagels, B. Kanngieer, M. Müller, B. Beckhoff, I. Grigorieva, A. Antonov, V. Arkadiev, and A. Bjeoumikhov, An efficient X-ray spectrometer based on

- thin mosaic crystal films and its application in various fields of X-ray spectroscopy, *J. Appl. Crystallogr.* **42**, 572 (2009).
- [26] E. J. Gamboa, D. S. Montgomery, I. M. Hall, and R. P. Drake, Imaging X-ray crystal spectrometer for laser-produced plasmas, *J. Instrum.* **6**, P04004 (2011).
- [27] T. Ebert, N. W. Neumann, T. Abel, G. Schaumann, and M. Roth, Laser-induced microstructures on silicon for laser-driven acceleration experiments, *High Power Laser Sci. Eng.* **5**, e13 (2017).
- [28] T. Ebert, R. Heber, T. Abel, J. Bieker, G. Schaumann, and M. Roth, Targets with cone-shaped microstructures from various materials for enhanced high-intensity laser-matter interaction, *High Power Laser Sci. Eng.* **9**, e24 (2021).
- [29] H. K. Chung, M. H. Chen, and R. W. Lee, Extension of atomic configuration sets of the Non-LTE model in the application to the $K\alpha$ diagnostics of hot dense matter, *High Energy Density Phys.* **3**, 57 (2007).
- [30] S. B. Hansen, A. Y. Faenov, T. A. Pikuz, K. B. Fournier, R. Shepherd, H. Chen, K. Widmann, S. C. Wilks, Y. Ping, H. K. Chung, A. Niles, J. R. Hunter, G. Dyer, and T. Ditmire, Temperature determination using $K\alpha$ spectra from M-shell Ti ions, *Phys. Rev. E* **72**, 036408 (2005).
- [31] J. Abdallah, R. E. Clark, A. Y. Faenov, L. Karpinski, S. A. Pikuz, V. M. Romanova, M. Sadowski, M. Scholz, and A. Szydlowski, Electron beam effects on the spectroscopy of multiply charged ions in plasma focus experiments, *J. Quant. Spectrosc. Radiat. Transf.* **62**, 85 (1999).
- [32] T. Kawamura, H. Nishimura, F. Koike, Y. Ochi, R. Matsui, W. Y. Miao, S. Okihara, S. Sakabe, I. Uschmann, E. Förster, and K. Mima, Population kinetics on $K\alpha$ lines of partially ionized Cl atoms, *Phys. Rev. E* **66**, 016402 (2002).
- [33] M. Šmíd, O. Renner, A. Colaitis, V. T. Tikhonchuk, T. Schlegel, and F. B. Rosmej, Characterization of suprathermal electrons inside a laser accelerated plasma via highly-resolved $K\alpha$ -emission, *Nat. Commun.* **10**, 4212 (2019).
- [34] X. Llovet, C. J. Powell, F. Salvat, and A. Jablonski, Cross sections for inner-shell ionization by electron impact, *J. Phys. Chem. Ref. Data* **43**, 013102 (2014).
- [35] P. Neumayer, B. Aurand, M. Basko, B. Ecker, P. Gibbon, D. C. Hochhaus, A. Karmakar, E. Kazakov, T. Kühl, C. Labaune, O. Rosmej, A. Tauschwitz, B. Zielbauer, and D. Zimmer, The role of hot electron refluxing in laser-generated K-alpha sources, *Phys. Plasmas* **17**, 103103 (2010).
- [36] O. Culfa, G. J. Tallents, E. Wagenaars, C. P. Ridgers, R. J. Dance, A. K. Rossall, R. J. Gray, P. McKenna, C. D. R. Brown, S. F. James, D. J. Hoarty, N. Booth, A. P. L. Robinson, K. L. Lancaster, S. A. Pikuz, A. Y. Faenov, T. Kampfer, K. S. Schulze, I. Uschmann, and N. C. Woolsey, Hot electron production in laser solid interactions with a controlled pre-pulse, *Phys. Plasmas* **21**, 043106 (2014).
- [37] H.-K. Chung, B. I. Cho, O. Ciricosta, S. M. Vinko, J. S. Wark, and R. W. Lee, Atomic processes modeling of x-ray free electron laser produced plasmas using SCFLY code, *AIP Conf. Proc.* **1811**, 020001 (2017).
- [38] G. Boutoux, N. Rabhi, D. Batani, A. Binet, J.-E. Ducret, K. Jakubowska, J.-P. Nègre, C. Reverdin, and I. Thfoin, Study of imaging plate detector sensitivity to 5-18 MeV electrons, *Rev. Sci. Instrum.* **86**, 113304 (2015).
- [39] A. L. Meadowcroft, C. D. Bentley, and E. N. Stott, Evaluation of the sensitivity and fading characteristics of an image plate system for x-ray diagnostics, *Rev. Sci. Instrum.* **79**, 113102 (2008).
- [40] M. Šmíd, X. Pan, and K. Falk, X-ray spectrometer simulation code with a detailed support of mosaic crystals, *Comput. Phys. Commun.* **262**, 107811 (2021).
- [41] G. Hölzer, O. Wehrhan, and E. Förster, Characterization of flat and bent crystals for x-ray spectroscopy and imaging, *Cryst. Res. Technol.* **33**, 555 (1998).
- [42] B. L. Henke, E. M. Gullikson, and J. C. Davis, X-ray interactions: Photoabsorption, scattering, transmission, and reflection at $E=50\text{-}30000$ eV, $Z=1\text{-}92$, *At. Data Nucl. Data Tables* **54**, 181 (1993).
- [43] L. C. Jarrott, A. J. Kemp, L. Divol, D. Mariscal, B. Westover, C. McGuffey, F. N. Beg, M. Suggit, C. Chen, D. Hey, B. Maddox, J. Hawreliak, H. S. Park, B. Remington, M. S. Wei, and A. Macphée, $K\alpha$ and bremsstrahlung x-ray radiation backlighter sources from short pulse laser driven silver targets as a function of laser pre-pulse energy, *Phys. Plasmas* **21**, 031211 (2014).